Supplementary Materials

Using InSAR Time Series to Monitor Surface Fractures and Fissures in the Al-Yutamah Valley, Western Arabia

Thamer Aldaajani [1,2,*], Mark Simons [1,3], Zhang Yunjun[1], David Bekaert [3], Khalid A. Almalki [2], and Yuan-Kai Liu [1]

[1] Seismological Laboratory, Division of Geological and Planetary Sciences, California Institute of Technology, Pasadena, CA, USA
[2] King Abdulaziz City for Science and Technology, Riyadh, Saudi Arabia
[3] Jet Propulsion Laboratory, California Institute of Technology, Pasadena, CA, USA
* Correspondence: thamer@caltech.edu

Regional phase residuals

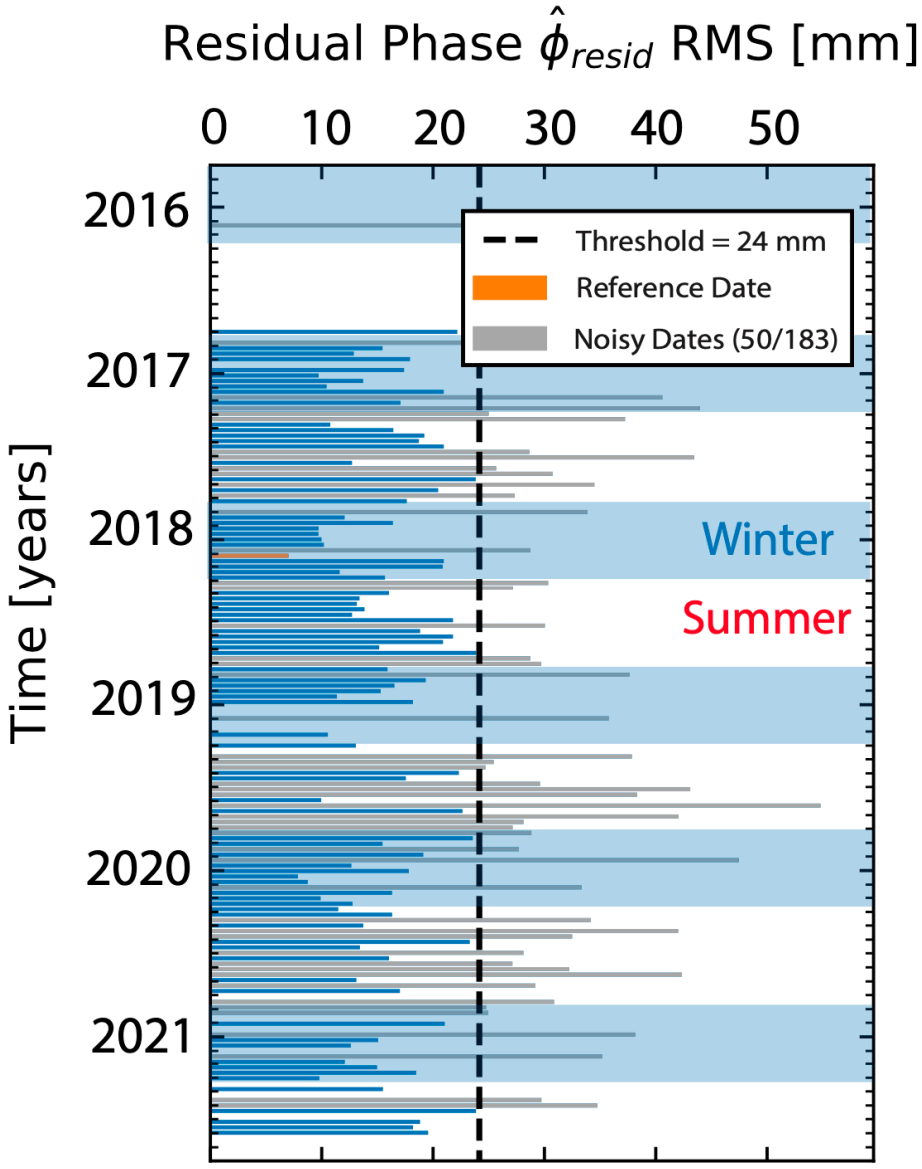

Figure S1: The RMS residuals for our regional analysis after removal of a temporal model that includes linear and periodic (annual and semiannual) components. We use a single threshold value to exclude acquisitions of particularly high residuals. Based on this analysis, we excluded 50 acquisitions out of 183.

Regional coherence history and interferogram network

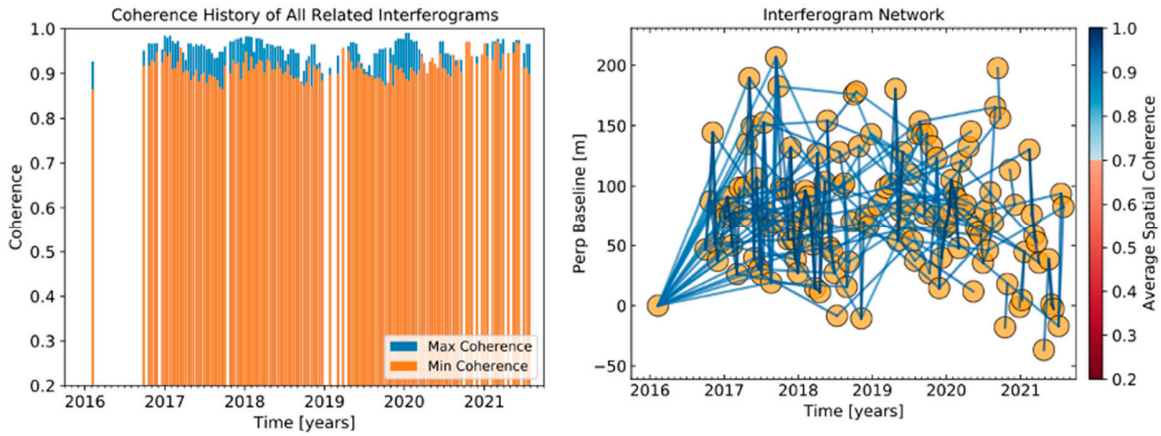

Figure S2: (Left) Coherence history at the regional scale. The average temporal coherence is above 0.8. (Right) Our interferogram network where the lines (i.e., pairs) are colored to indicate average spatial coherence.

Regional spatial and temporal solid earth tides

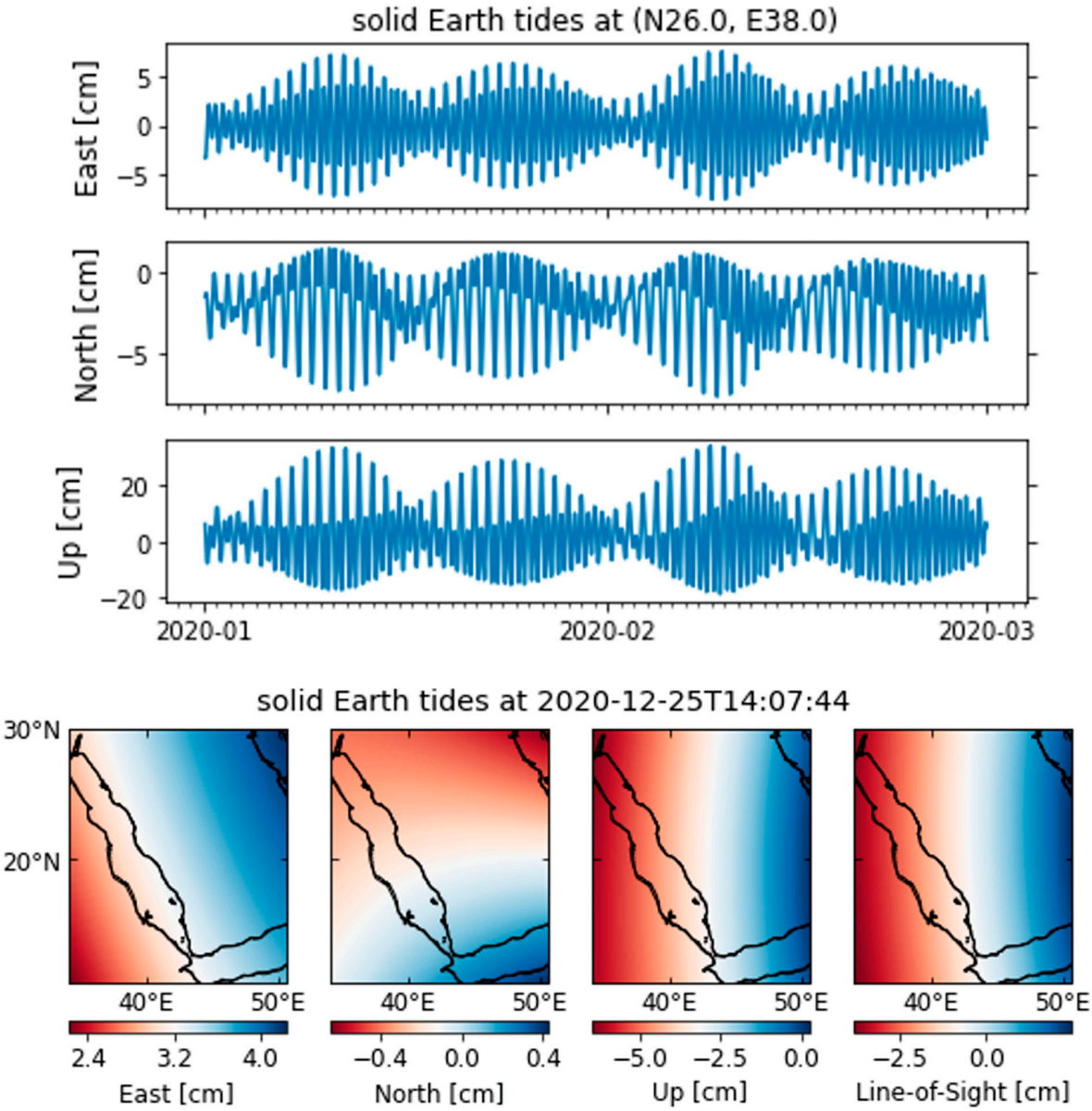

Figure S3: (Upper panel) Example of the solid earth tides as a function of time at the location [26N, 38E] for the period between 01/2020 until 03/2020 as calculated using the algorithm described in Milbert (2018). The vertical component is systematically the largest. (Lower panel) Instantaneous map of solid earth tides for western Arabia on 12/25/2020 at 14:07:44 GMT. The large predicted effect in the LOS component is shown at the far right.

Velocity field of western Arabia after removing solid earth tides

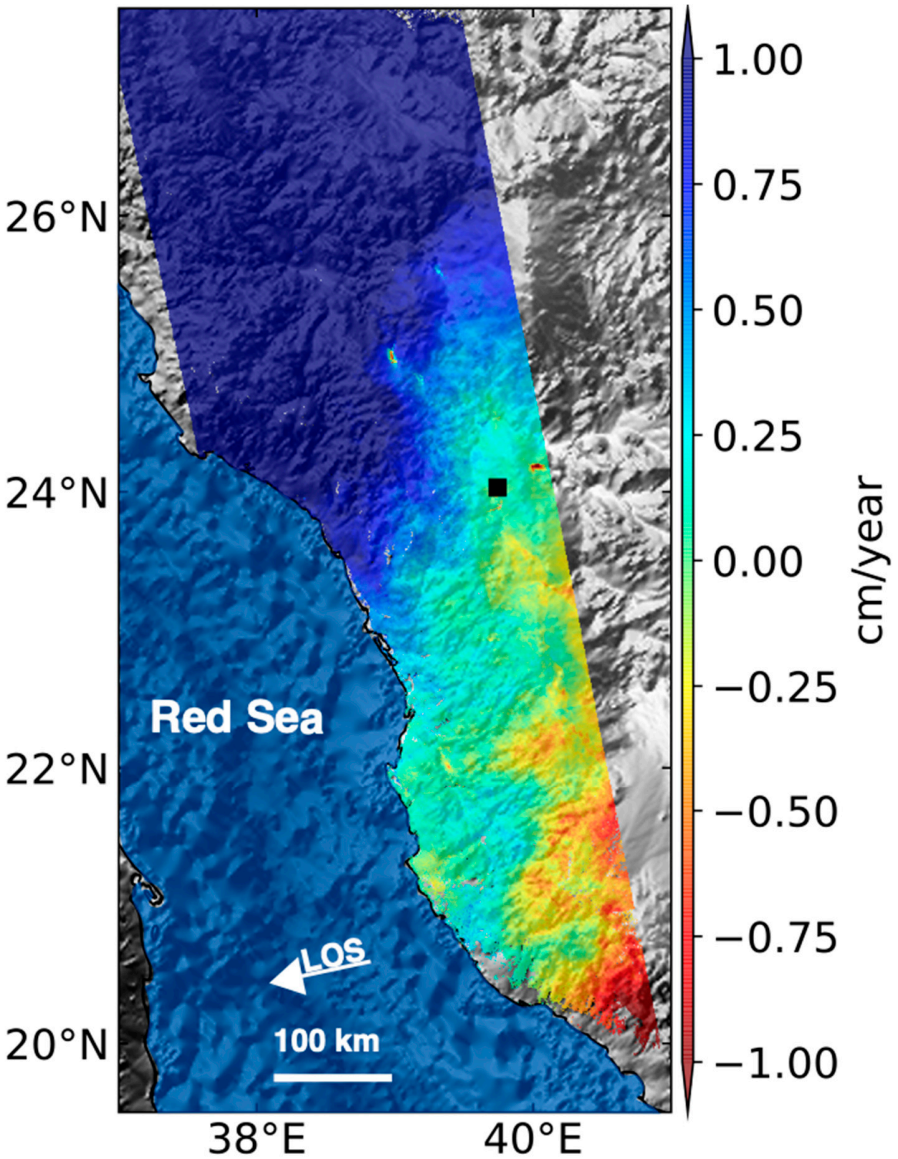

Figure S4: The velocity field of western Arabia after removing the phase residual corresponding to the solid earth tides. A long wavelength component is still visible. Black square denotes spatial reference. White arrow shows the radar looking direction relative to the ground.

Velocity field of western Arabia after removing delay due to troposphere

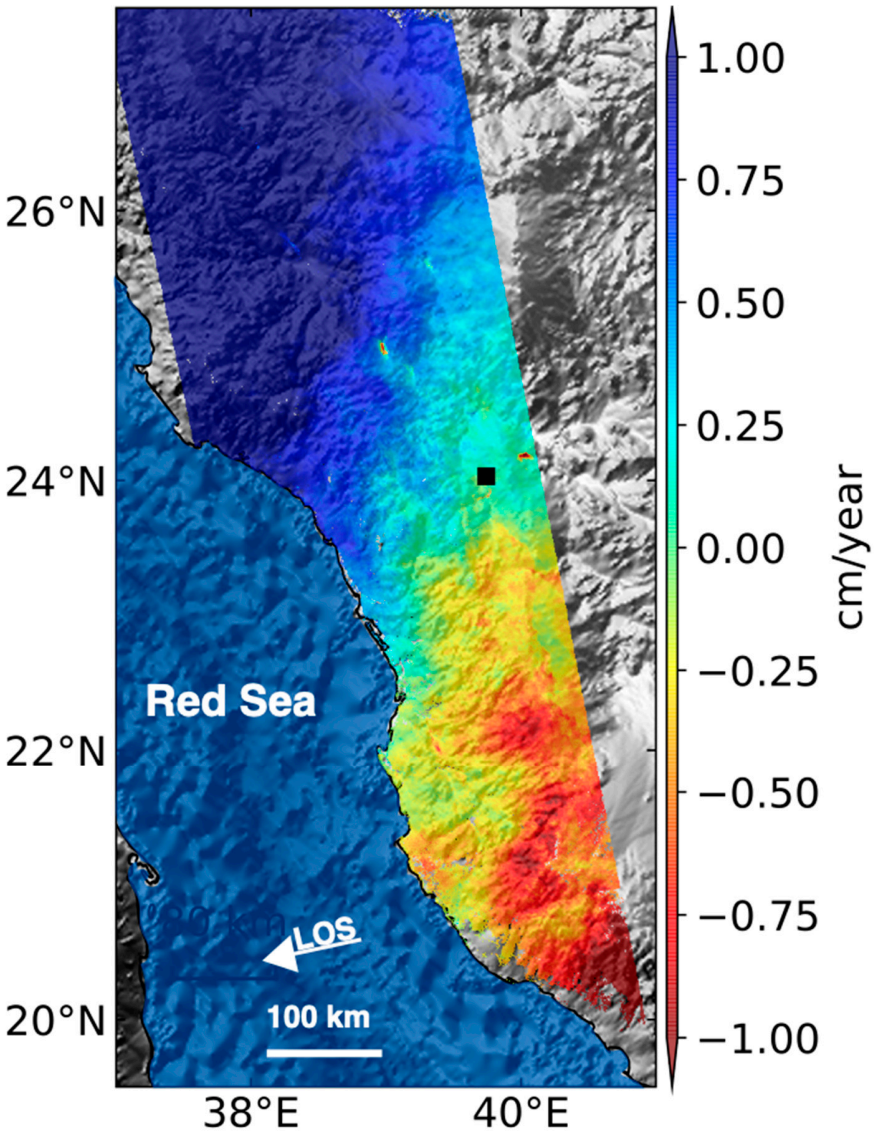

Figure S5: The velocity field of western Arabia after removing the phase residual corresponding to the effects due to temporal variations in the quasi-stratified component of the troposphere. A long wavelength residual remains. Black square denotes spatial reference. White arrow shows the radar looking direction relative to the ground.

Velocity field of western Arabia after removing effect of DEM error

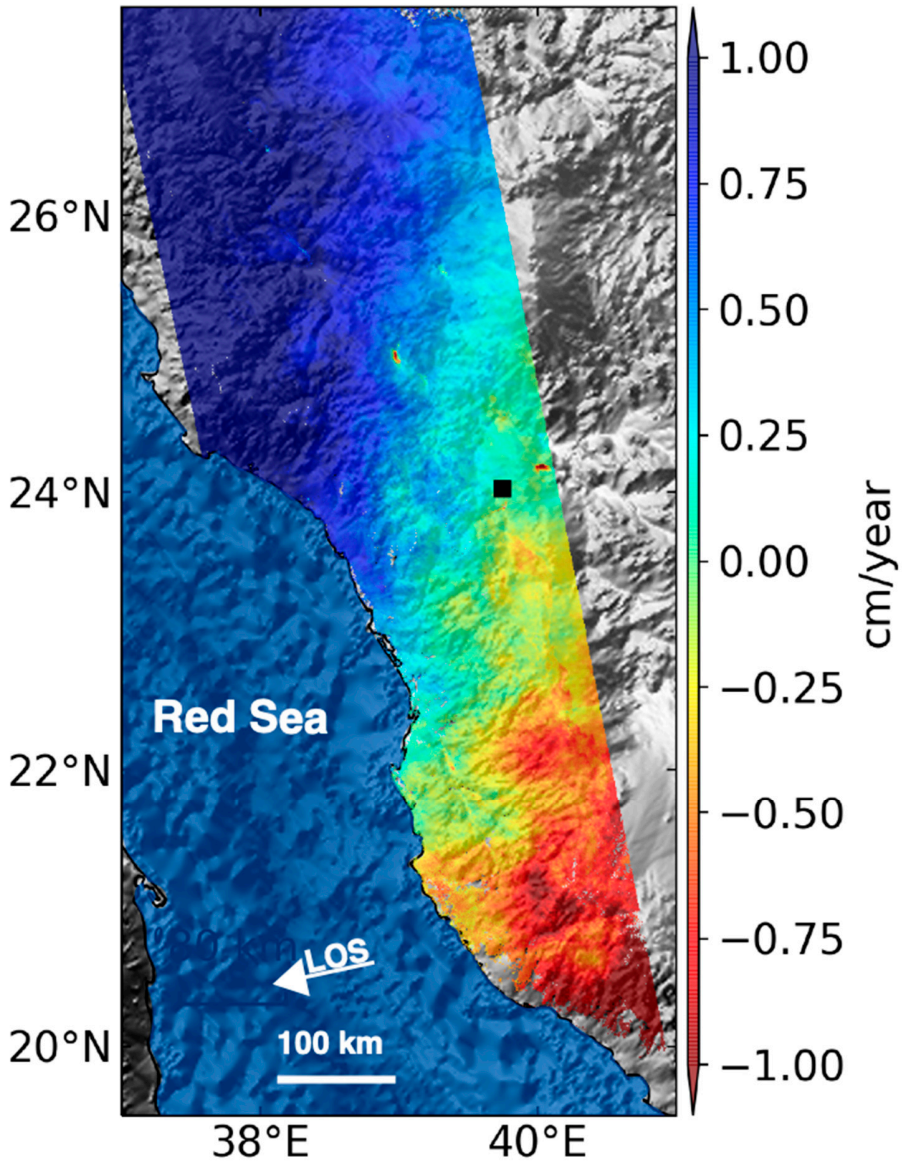

Figure S6: The velocity field of western Arabia after removing the phase residual corresponding to the DEM error. As we use the small baseline acquisition strategy with low sensitivity to topography, we do not expect to see any significant changes. Black square denotes spatial reference. White arrow shows the radar looking direction relative to the ground.

Spatial distribution of annual periodic signal

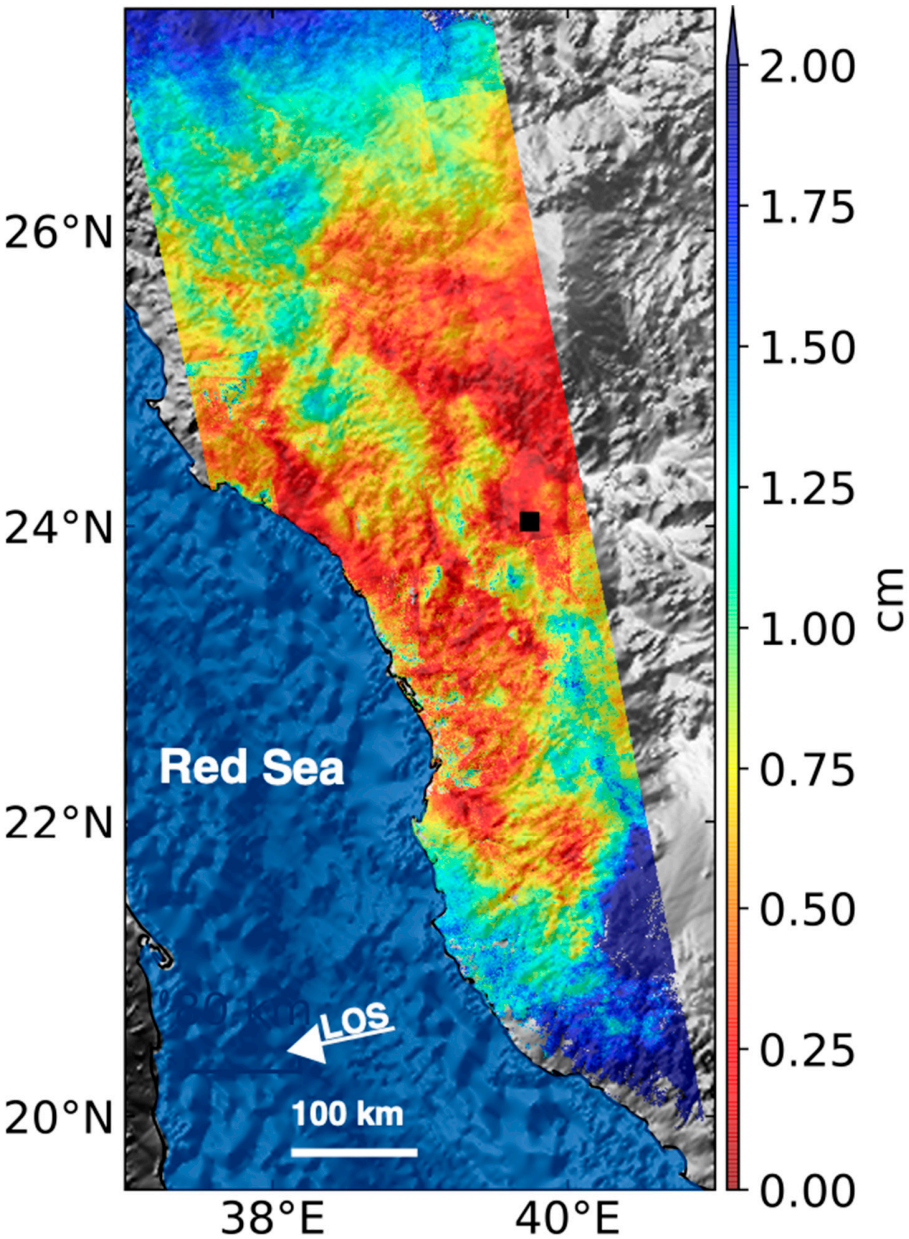

Figure S7: The spatial distribution of the magnitude of the annual periodic signal as estimated from our InSAR time series for the period between 01/2016 until 09/2021. This map demonstrates that the annual magnitude reaches its maximum peaks in the southern and northern ends of our regional coverage. Black square denotes spatial reference. White arrow shows the radar looking direction relative to the ground.

Spatial distribution of semi-annual periodic signal

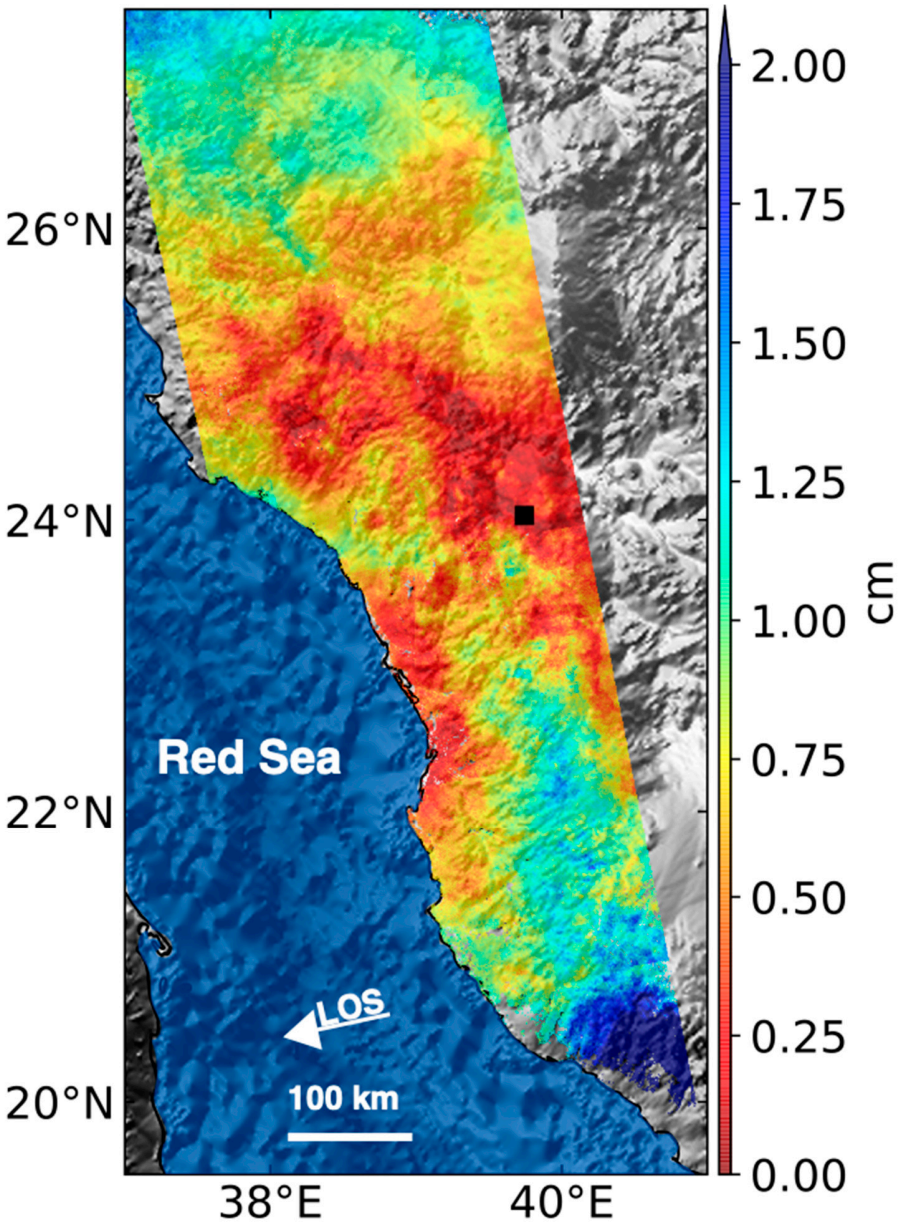

Figure S8: The spatial distribution of the magnitude of the semi-annual component as estimated from our InSAR time series for the period between 01/2016 until 09/2021. We can see lower magnitudes in comparison to the annual signal. Black square denotes spatial reference. White arrow shows the radar looking direction relative to the ground.

Spatial distribution of error

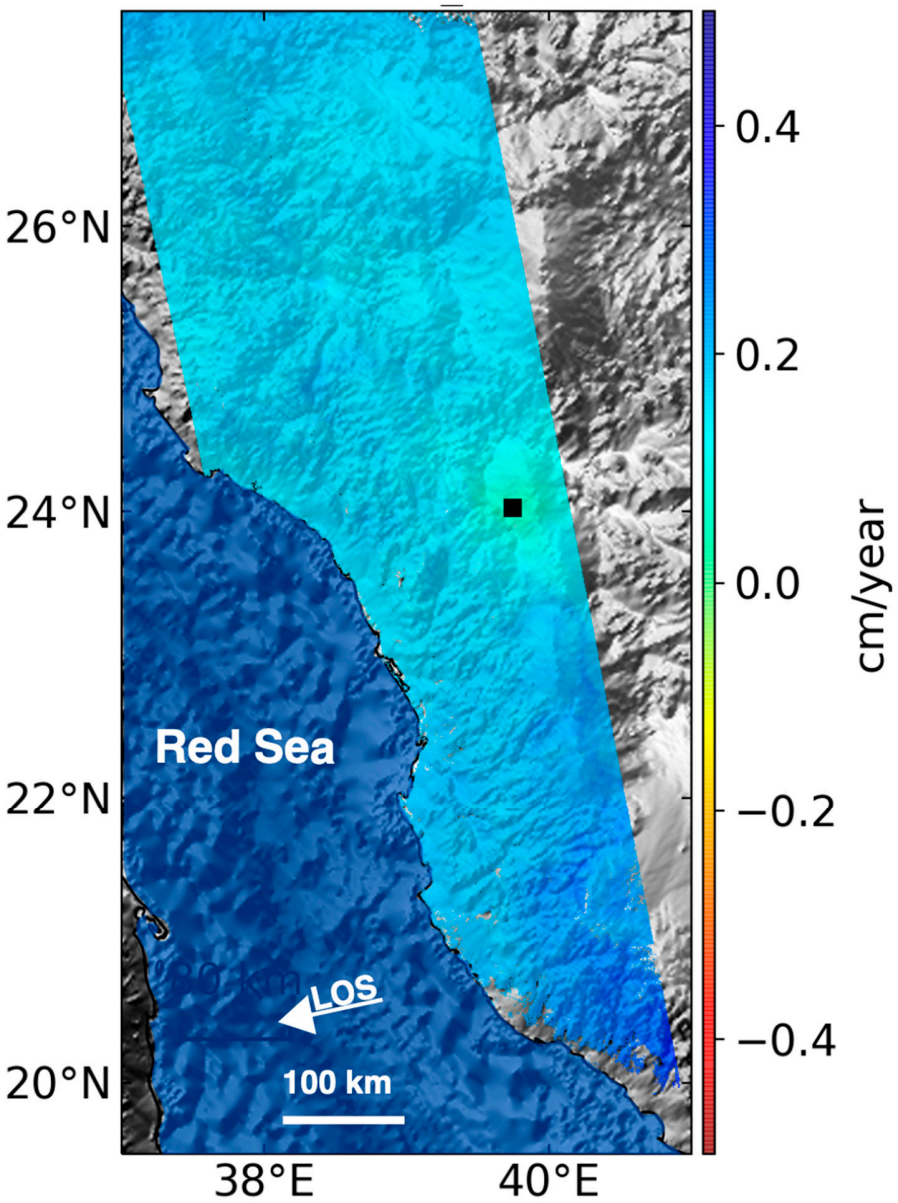

Figure S9: The standard deviation of the velocity map shown in figure 2. The error increases as a function of distance from the reference point (black quadrangle). The error is relatively low throughout. Black square denotes spatial reference. White arrow shows the radar looking direction relative to the ground.

Local phase residuals

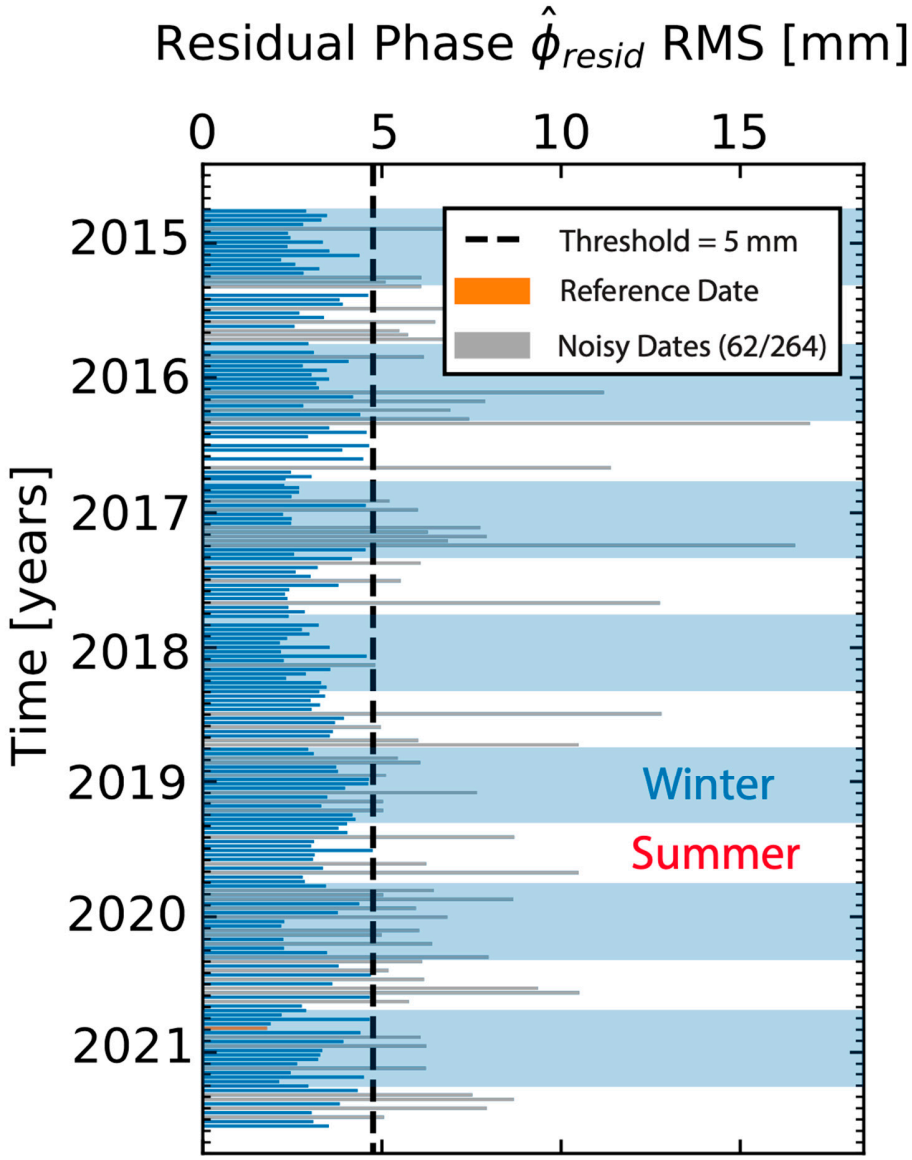

Figure S10: The RMS residuals for our local analysis. We use a 5 mm threshold to remove particularly noisy acquisitions. Based on this analysis, we excluded 62 acquisitions out of 264. There is no persistent pattern that can be seen in the figures.

Local coherence history and interferogram network

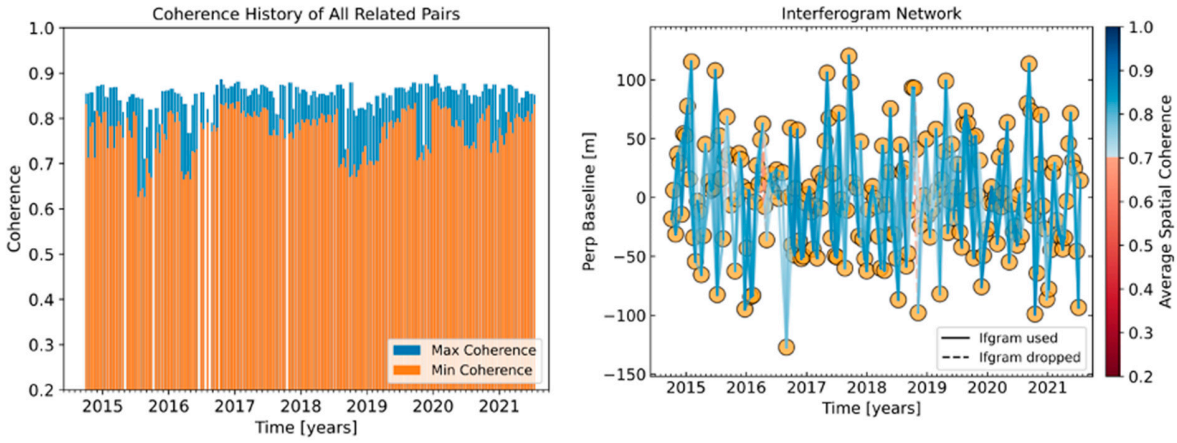

Figure S11: (Left) The coherence history averaged for the Al-Yutamah Valley. The average temporal coherence fluctuates between 0.6-0.85. (Right) Our interferogram network for the local high resolution analysis, which is less redundant in comparison with the regional analysis.

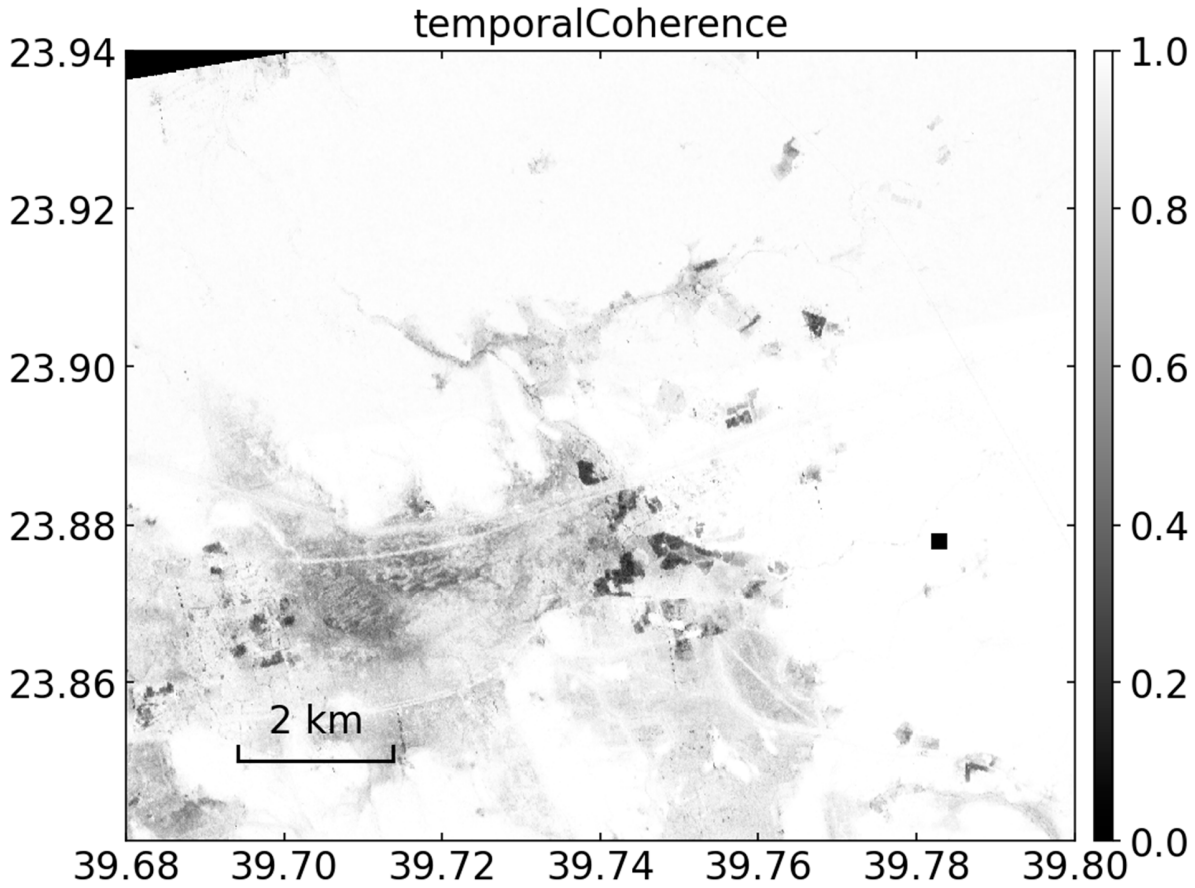

Figure S12: Impact of network modification on temporal coherence for Sentinel-1 dataset. This figure shows the temporal coherence for the Al-Yutumah valley as obtained by inverting a network of small baseline interferograms using uniform weighting. Low coherence domains are correlated with regions of agricultural activities. Black square denotes spatial reference.

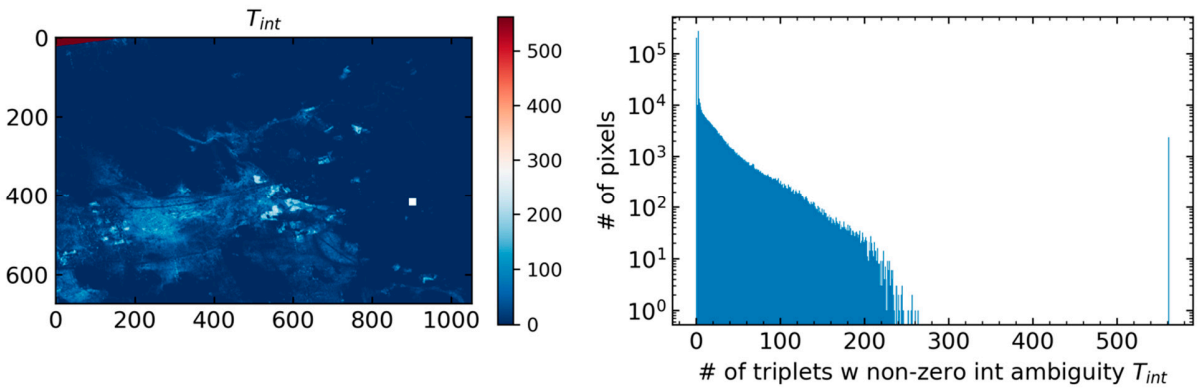

Figure S13 (Left) Map and (Right) histogram of number of triplets with non-zero phase closure generated from 580 interferograms and 202 Sentinel-1 acquisitions. The spikes indicate that the majority of pixel are unwrapping error free. Black square (Left) denotes spatial reference.